Available online at www.sciencedirect.com
ScienceDirect
Journal of the European Ceramic Society 31 (2011) 2339–2349
www.elsevier.com/locate/jeurceramsoc

Effect of commercial anatase-TiO_2 raw materials on the electrical characteristics of ceramics with positive temperature coefficient of resistivity

K. Kirstein [a], K. Reichmann [a,*], W. Preis [b], S. Mitsche [c]

[a] *Institute for Chemistry and Technology of Materials, Graz University of Technology, Stremayrgasse 9, 8010 Graz, Austria*
[b] *Chair of Physical Chemistry, University of Leoben, Franz-Josef-Straße 18, 8700 Leoben, Austria*
[c] *Austrian Centre for Electron Microscopy and Nanoanalysis, Institute of Electron Microscopy and Fine Structure Research, Steyrergasse 17, Graz University of Technology, 8010 Graz, Austria*

Received 3 December 2010; received in revised form 20 April 2011; accepted 5 May 2011
Available online 1 July 2011

Abstract

Cause and effect of commercially available anatase-TiO_2 on the positive temperature coefficient of resistivity (PTCR) characteristics of donor- and acceptor-codoped (Ba,Ca)TiO_3-ceramics have been investigated. Compositions containing several anatase raw materials have been studied by means of scanning electron microscopy, in particular EDXS/WDXS-techniques, as well as electron backscattering diffraction (EBSD) and impedance spectroscopy. It is clearly shown that the crystallographic modifications rutile and anatase are replaceable without any significant effect on the PTCR-characteristics, if these raw materials have similar physical and chemical properties such as grain size distribution, specific surface area and impurity content. Further it is demonstrated that the impurities of commercial anatase powders, which are a result of preparation conditions, strongly affect the electrical properties. By use of impedance analysis and electron backscattering diffraction we conclude that the differences in PTCR-characteristics can be attributed to the grain boundary region due to dopant distribution and segregative additive effects and not to microstructural modifications.

Keywords: TiO_2; Impurities; $BaTiO_3$ and titanates; PTC devices; Impedance spectroscopy; Scanning electron microscopy

1. Introduction

Oxide semiconductors exhibiting a positive temperature coefficient of resistivity (PTCR) are mainly based on modified barium titanate compositions, which enable a wide temperature range of application. In overload protection, as heating elements or simple thermostatic switches these PTCR components are a mass product counted in several hundred tons per year.[1–4] Some applications require enhanced PTCR characteristics, i.e. steeper or higher PTCR-jumps. Such materials can be obtained by means of codoping the n-conducting $BaTiO_3$ with acceptor ions such as Mg or Mn.[5–8] This article focuses on such donor- and acceptor-codoped (Ba,Ca)TiO_3 prepared from different titanium dioxide raw materials.

Commercially, rutile and anatase raw materials are produced via two wet chemical routes that is to say the sulfate process mainly producing the metastable anatase modification and the chloride process resulting in the thermodynamically stable rutile form. Both methods were already established in the 1940s and were described in detail and published by Barksdale.[9] Additionally, several other processes are known to generate anatase or rutile on a laboratory scale.[10–13] Later investigations showed that anatase materials are always contaminated at the grain surfaces in order to stabilise the metastable form hence resulting in higher impurity contents depending on the preparation and refinement conditions.[14–16] The use of commercial anatase TiO_2 was discussed because this modification is a cheap mass product, which is found in paints and fillers. The main impurities of this type of material are potassium and phosphorus in the range of several hundred ppm. Empirical observations have shown that the use of anatase for the production of PTCR thermistors is not possible, although no satisfying scientific explanation has been available yet.[17]

Commonly $BaTiO_3$ based PTCR-materials are produced in a large scale via a modified solid-state-synthesis route that is well investigated since the 1960s.[4,5,18] Kinetic studies on the solid

* Corresponding author. Tel.: +43 316 873 32321; fax: +43 316 873 1032321.
E-mail address: k.reichmann@tugraz.at (K. Reichmann).

0955-2219/$ – see front matter © 2011 Elsevier Ltd. All rights reserved.
doi:10.1016/j.jeurceramsoc.2011.05.028

state synthesis using both anatase and rutile were carried out by several authors revealing that the reactivity of the TiO_2 material during $BaTiO_3$ formation is determined by the raw material properties, namely grain size distribution, specific surface area, pre-treatment of the raw material and the type and quantity of impurities, the latter primarily affecting the secondary phase formation during synthesis.[19–28]

The PTCR effect is known to occur only in n-conducting $BaTiO_3$ that can be obtained by doping the isolating $BaTiO_3$ with tri- or pentavalent ions, which substitute for barium and titanium respectively. Typical raw materials for the production of PTCR thermistors are Ba-, Ca-, Sr- and/or Pb-carbonates and high purity rutile TiO_2 as well as doping additives such as La, Dy and Nb added as solution of e.g. chlorides or acetates in concentrations between 0.1 and 1.0 at.%. Intensive research was performed to elucidate the effects of rare earth doping in $BaTiO_3$ on the performance of the PTCR ceramics. Such compositions always show a maximum conductivity at characteristic doping concentrations.[6,7,29–31] Widely accepted models to explain the resistivity temperature characteristic in n-$BaTiO_3$ are the Heywang- and Jonker-model, both reviewed elsewhere.[4] While the Heywang model is suitable to describe the R–T behavior above the Curie temperature (T_C), the Jonker model fits below T_C. It is also well known that the characteristic ferroelectric–paraelectric phase transition at T_C, which occurs around 120 °C in pure $BaTiO_3$, can be shifted towards lower or higher temperatures by substituting barium with strontium or lead respectively.[4,32,33] Additionally, the slope and height of the PTCR-jump can be enhanced by codoping n-$BaTiO_3$ with acceptor ions such as magnesium or manganese which both substitute for titanium.[5–8] The same can be gained by adding sintering aids such as SiO_2, B_2O_3 or excess TiO_2 which support liquid phase generation and influence dopant distribution simultaneously.[34–37]

Moreover, process parameters such as sintering temperature, sintering atmosphere and cooling conditions have to be taken into account, each influencing the formation of the potential barrier which is located at the grain boundaries and originates the PTCR in n-conducting barium titanate.[4,5,18,38–40]

Finally an assumption should be made about the influences of the main impurities phosphor and potassium, which are present in the anatase raw materials, on the PTCR-characteristics in n-(Ba,Ca)TiO_3. It is supposed that the addition of phosphor provokes liquid phase generation due to its ability to act as a glass network former[41,42] but alternatively it must be taken into account that the P^{5+} ion might be incorporated into the $BaTiO_3$ lattice substituting for Ti^{4+} hence acting as donor dopant ($P_{Ti}^{\bullet}$).[43–46] Additionally, similar assumptions can be made in case of potassium which might act as glass network modifier influencing the liquid phase properties[41,42] or substitute for Ba^{2+} thus acting as acceptor dopant (K'_{Ba}). The latter assumption especially is valid for impurity ions, which are able to substitute for barium or titanium by reason of the ionic radii, as is the case for phosphor and potassium. Finally it is important to note that alkaline metals such as potassium tend to volatilize under temperature load (alkali volatility) especially at temperatures above 1000 °C.[41]

Due to the insufficient understanding about the effects of anatase-TiO_2 on the electrical characteristics of PTCR components, the aim of this work is to clarify the role of anatase raw materials on the electrical properties of donor- and acceptor-codoped (Ba,Ca)TiO_3 and verify the presumptions introduced above.

2. Materials and methods

2.1. Raw material characterization

Four different types of TiO_2 raw materials were used to study the effect of anatase in preparation of PTCR materials: anatase no.1 (A-1), a commercially available material with specific surface area (BET) of 10.3 m^2/g, anatase no.2 (A-2) with specific surface area of 9.4 m^2/g, anatase–rutile mixture no.1 (A/R-1) containing about 89 wt.% anatase and 11 wt.% rutile and having a specific surface area of 14.3 m^2/g, and contrarily anatase–rutile mixture no.2 (A/R-2) containing about 9 wt.% anatase and 91 wt.% rutile with specific surface area of 10.2 m^2/g. Both anatase materials (A-1 and A-2) were manufactured by the sulfate process. The materials A/R-1 and A/R-2 were produced from chloride process. Finally, as a reference material, commercially available rutile (R-1) as well produced from sulfate process with specific surface area of 6.1 m^2/g is used. Table 1 summarizes relevant properties and parameters of the TiO_2 raw materials mentioned.

It is evident from Table 1 that both anatase materials prepared from sulfate process (A-1 and A-2) contain a higher amount of total impurities compared to the rutile reference (R-1). The main impurities in A-1 and A-2 are phosphor and potassium with an amount of approximately 0.3 wt.% in A-2 and 0.2 wt.% in A-1. In contrast phosphor and potassium amounts less than 0.01 wt.% in both the rutile reference and the rutile–anatase mixture materials.

The other raw materials used were high purity barium carbonate with average grain size of 1.5 μm and specific surface of 1.8 m^2/g as well as calcium carbonate with average grain size of 3.5 μm and specific surface of 2.5 m^2/g (Solvay Bario E Derivati SpA). The main impurities in both carbonates are $SrCO_3$ with a maximum content of 0.17 wt.% and Na_2CO_3 with a maximum content of 0.03 wt.%. Yttrium is added as donor dopant (Treibacher Auermet Produktions GmbH) and manganese is selected as acceptor dopant (Lactan Chemikalien und Laborgeräte Vertriebsgesellschaft m.b.H. & Co. KG), both processed as acetate solutions.

2.2. Sample preparation

Two series of compositions (a and b) with varying titanium excess ranging from 0.002 mol% for series a to 0.015 mol% for series b were prepared from above listed raw materials. The amounts of dopants are fixed at the level of 0.5 mol% yttrium and 0.1 mol% manganese with respect to the barium content. Additionally, about 1 mol% SiO_2 is added to the compositions to improve liquid phase sintering. In Table 2 the compounds are listed by molar compositions.

Table 1
Properties of the titanium dioxide raw materials.

General information	Labelling Producer Modification	A-1 Cerac Inc. Anatase	A-2 Kronos Intern. Inc. Anatase	R-1 Tronox Inc. Rutile	A/R-1 Tronox Inc. Anatase/rutile mixture	A/R-2 Tronox Inc. Rutile/anatase mixture
BET	(m^2/g)	9.38	10.31	6.06	14.25	10.17
Impurities ICP-quantity [ppm]	Na	45.10	44.80	14.89	2.92	1.70
	Mg	14.22	3.80	2.86	n.d.	n.d.
	Al	53.05	18.56	12.38	0.27	0.00
	P	863.58	1019.16	42.37	35.02	30.30
	K	1261.20	1716.90	21.86	0.00	0.00
	Cl	n.d.	n.d.	n.d.	227.00	255.00
	Fe	6.14	4.58	6.22	7.52	4.50
	Zr	98.96	26.87	123.82	n.d.	n.d.
	Nb	111.59	101.08	79.47	2.22	3.11
Total	(wt.%)	0.245	0.294	0.030	0.027	0.029

The raw materials are homogenized in deionised water using a ball mill with yttria-stabilised zirconia (YSZ) spheres 3.0 mm in diameter followed by drying at 90 °C in a drying chamber for at least 48 h. Afterwards the homogenized mixture is calcined in a batch furnace in air at a temperature of 1190 °C for 5 h. The calcined powder is then milled in deionised water, again by using a ball mill with YSZ spheres of 3.0 mm, until a final grain size of 2.5–2.8 μm (d_{50}) is obtained. For spray drying 3 wt.% of a cellulose binder mixture is added. Subsequently the granulated material is compacted by means of an axial moulding press to pellets with a shape of 14.4 mm in diameter and 3.15 mm in height. The resulting green density of the compressed pellets amounts to 3.15 g/cm^3. Green parts finally are sintered in a batch furnace at 1350 °C with dwell time of 30 min and a cooling rate of 5 K/min.

2.3. Measurement techniques

For electrical characterization the sintered parts were metalized by first supplying a chromium/nickel-sputter layer and finally screen printing the sputtered parts with silver electrodes.

The resistivity at 25 °C (ρ_{25}) was measured by using a digital multimeter Keithley 199 (Keithley Instruments Inc.) with a working range up to 300 MΩ (measurement current 1.7 mA to 0.5 μA). The ρ–T characteristic was recorded between 30 °C and 280 °C in air by means of a test assembly containing the source measure unit Keithley 237, the switch system Keithley 7001 (Keithley Instruments Inc.) and the air convection oven Memmert UFE 400 (Memmert GmbH & Co. KG). The measurement voltage was fixed at 1 V.

In addition calcined powders and sintered samples were examined by X-ray diffraction using a Siemens D5005 (Bruker AXS) diffractometer with Cu-Kα-radiation, diffracted beam graphite monochromator and scintillation counter detector. Typical measurement parameters used are a source voltage of 40 kV, measurement current of 30 mA and a 2Θ-range between 20° and 60° with step size of 0.02°. No significant differences in lattice parameters (c/a axis ratio) and composition could be detected (Table 3).

2.4. Scanning electron microscopy

Cross sections of the sintered pellets were embedded in epoxy resin and ground and polished. Finally, the specimens were polished with an alkaline colloidal silica solution (OP-U suspension from Struers, 0.04 μm granularity) for 60 min. This preparation procedure was necessary in order to perform electron backscatter diffraction (EBSD). Additionally, these specimens were used for wavelength and energy dispersive X-ray spectrometry (WDXS and EDXS). The EDXS, WDXS and EBSD analyses were accomplished on a Zeiss Ultra 55 FESEM equipped with a Trident system from the EDAX Company. The Trident system comprise a Sapphire Si(Li) EDX detector and a TEXS WDX spectrometer for element analyses and a CCD-digiview-camera

Table 2
Molar compositions of the investigated batches.

Batch no.	TiO_2 labelling	Composition (mol%)				Dopant	A/B ratio
		$BaCO_3$	$CaCO_3$	TiO_2	SiO_2		
A-1a	A-1	42.20	7.50	49.98	0.99	Y/Mn	0.998
A-2a	A-2	42.20	7.50	49.98	0.99	Y/Mn	0.998
R-1a	R-1	42.20	7.50	49.98	0.99	Y/Mn	0.998
A-1b	A-1	42.20	7.50	50.64	0.98	Y/Mn	0.985
A-2b	A-2	42.20	7.50	50.64	0.98	Y/Mn	0.985
R-1b	R-1	42.20	7.50	50.64	0.98	Y/Mn	0.985
A/R-1b	A/R-1	42.20	7.50	50.64	0.98	Y/Mn	0.985
A/R-2b	A/R-2	42.20	7.50	50.64	0.98	Y/Mn	0.985

Table 3
Phase composition of the calcined powders detected by X-ray diffraction.

Batch no.	Phase composition (wt.%)				*c*/*a* axis ratio
	$(Ba,Ca)TiO_3$	$CaTiO_3$	$Ba_6Ti_{17}O_{40}$	$Ba_2TiSi_2O_8$	
A-1a	93.7	3.6	2.8	n.d.	1.010
A-2a	94.2	3.4	2.5	n.d.	1.010
R-1a	94.1	3.5	2.4	n.d.	1.011
A-1b	91.8	4.3	2.4	1.5	1.011
A-2b	90.1	2.6	n.d.	0.9	1.010
R-1b	92.8	4.5	1.9	0.9	1.011
A/R-1b	91.9	4.8	2.1	1.2	1.011
A/R-2b	92.2	4.4	2.3	1.2	1.011

for EBSD. The EDXS and WDXS data were recorded and evaluated with the Genesis software V6.1, the EBSD data with OIM 5.3 software. The operation conditions (high voltage and beam current) for EDXS were 15 kV and 1.5 nA, for WDXS 20 kV and 30 nA. During the EBSD characterization the microscope was operated at 20 kV and 1.8 nA and an area of 100 μm × 100 μm was scanned with a step size of 100 nm (hexagonal pixels). Grain boundaries were characterized by a misorientation larger than 5° between neighbouring measurement points. To reduce the influence of noise in the results, a grain must comprise at least six pixels, which results in a minimum grain diameter of around 0.4 μm.

2.5. Impedance spectroscopy

Impedance measurements were performed on disk-shaped samples (diameter: 12 mm, thickness: 2.5 mm) in air at temperatures between room temperature and 110 °C by employing a high-precision impedance analyzer (Novocontrol Alpha-A). The effective ac voltage amounted to 1.0 V and the frequency range was from 10 MHz to 100 mHz. The specimens were placed in the sample holder between two gold foils by light spring action. The stray inductance of the leads of the measurement jig was determined on the empty short-circuited sample holder. The AC measurements were carried out in a tube furnace equipped with a temperature controller (Eurotherm 2416) and the temperature was recorded in the vicinity of the sample by type-K thermocouples.

3. Results

3.1. Specific resistance and ρ–T-characteristics

Fig. 1 depicts the measured resistivity (ρ_{25}) values of all compositions at room temperature. It can be seen that compounds containing anatase TiO_2 prepared from the sulfate process lead to much higher resistivity values ranging from 3×10^5 to 2×10^6 Ω cm for compositions A-1a and A-2a (A/B-ratio 0.998) and 1.4×10^3 to 2.7×10^3 Ω cm for compositions A-1b and A-2b (A/B-ratio 0.985) which are 2–4 orders of magnitude higher than the rutile references R-1a and R-1b showing resistivity values of about 123 and 33 Ω cm respectively.

In contrast the anatase–rutile mixture materials A/R-1b and A/R-2b (A/B ratio 0.985) do not show any significant changes in room temperature resistivity compared to the rutile reference R-1b. The resistivity values obtained with these raw materials range between 25 Ω cm and 23 Ω cm, which is quite close to the reference value of 33 Ω cm achieved for composition R-1b. It is also evident from Fig. 1 that the use of anatase raw materials with higher impurity level significantly increases the standard deviation of the resistivity.

The PTCR-characteristics of the compositions prepared are illustrated in Fig. 2. It is obvious that anatase-materials show PTCR-characteristics as well, although the shape changes especially with regard to the slope and height of the PTCR-jump and the characteristic temperatures (temperature of minimum and maximum resistance, onset-temperature). Compared to the rutile reference the maximum resistivity (ρ_{max}) and the maximum temperature (T_{max}) respectively are shifted towards lower temperatures when using sulfate-processed anatase as the TiO_2 source (compositions A-1 and A-2 compared to R-1). It is also visible from Fig. 2 that changing the A/B-ratio towards higher Ti-excess leads to a shift of the room temperature resistivity respectively ρ_{min} towards lower values which is consistent with the literature.[47–49] On the contrary, the PTCR characteristic of the compositions prepared from anatase–rutile mixture materials (A/R-1 and A/R-2) do not show any significant changes compared to the rutile reference. Additionally, Fig. 3 represents the resulting values for $\Delta\rho/\Delta T$, i.e. the slopes of the PTCR-jump plotted against temperature. One characteristic point therein is

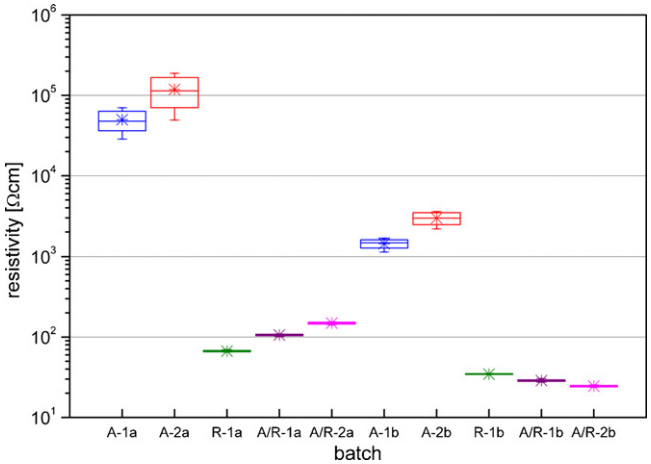

Fig. 1. Box plot of the resistivity at room temperature of series a- and b-compositions.

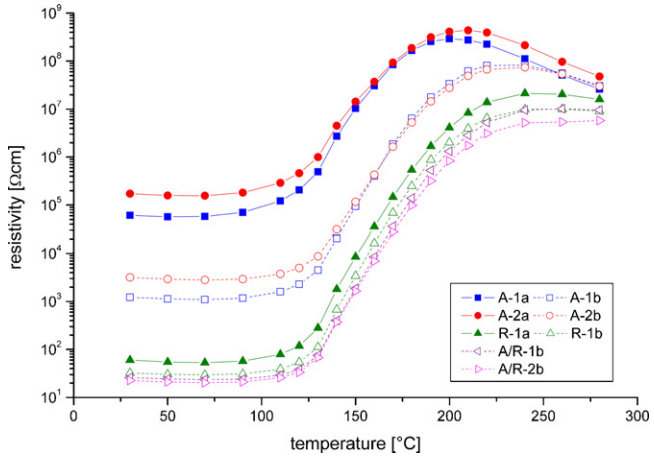

Fig. 2. Resistivity as a function of temperature (ρ–T-characteristic) of series a- and b-compositions.

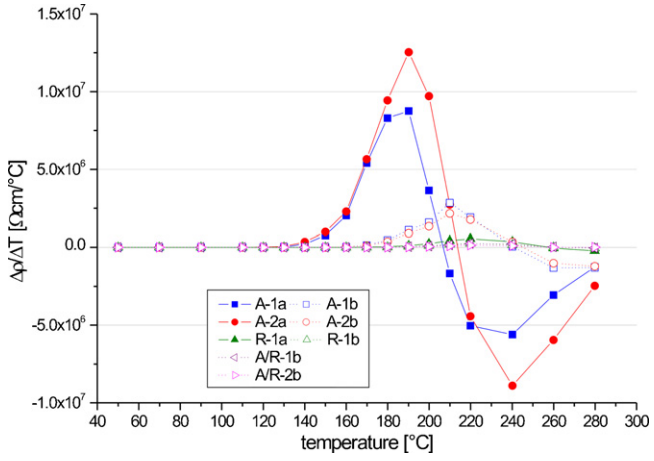

Fig. 3. Plot of $\Delta\rho/\Delta T$ as a function of temperature for a- and b-compounds.

the reversal from positive to negative alpha values representing T_{max}. For better comparison, Table 4 summarizes the characterizing values ρ_{min}, ρ_{max}, T_{max} and alpha (130–180 °C) of series a- and b-compositions. It is apparent from Fig. 3 and Table 4 that the rutile reference composition (R-1) as well as the anatase–rutile mixture compositions (A/R-1, A/R-2) show very flat $\Delta\rho/\Delta T$ vs. T curves resulting in higher T_{max} whereas the compositions prepared from anatase (A-1, A-2) show much steeper $\Delta\rho/\Delta T$ vs. T graphs and for this reason lower T_{max}. Moreover it is obvious

Table 4
Characteristic values of the ρ–T-graph.

Batch no.	ρ_{min} (Ω cm)	ρ_{max} (Ω cm)	T_{max} (°C)	$\alpha_{(130–180\,°C)}$ (%/°C)
A-1a	5.7E+04	2.9E+08	200	11.67
A-2a	1.6E+05	4.4E+08	209	10.49
R-1a	5.3E+01	2.1E+07	247	15.16
A-1b	1.1E+03	8.2E+07	240	14.56
A-2b	2.8E+03	7.4E+07	233	12.85
R-1b	2.9E+01	1.0E+07	252	15.45
A/R-1b	2.4E+01	1.0E+07	257	15.08
A/R-2b	2.0E+01	5.8E+06	253	14.59

that higher Ti-excess results in flatter $\Delta\rho/\Delta T$ vs. T curves once again correlated with an increase in T_{max}.

3.2. Microscopic studies

To clarify the chemical phase evolution especially the locations where phosphorus and potassium are incorporated, microscopic investigations were performed by EDXS and WDXS, as described in Section 2.3. Exemplary for both commercial anatase materials (A-1 and A-2), relevant EDX- and WDX-spectra of anatase composition A-2 compared to rutile composition R-1 and their location within the microstructure of the sintered parts are shown in Fig. 4a–c. Expected main and minor phases, which are typical for n-conducting (Ba,Ca)TiO_3 ceramics could clearly be detected. These are at first the main phase (Ba,Ca)TiO_3 representing the grain composition, second a titanium rich minor phase located in the grain interspaces representing the $BaTiO_3$–$Ba_6Ti_{17}O_{40}$ eutectic phase and third a silicon containing minor phase likewise located between the grains representing the liquid phase generated during sintering due to SiO_2 addition. These results indicate that the chemical evolution of both compositions is similar with respect to the expected main and minor phases. Furthermore the EDX-spectrum in Fig. 4b (region 1) compares another minor phase, which was identified as $CaTiO_3$. This minor phase contains extraordinary high yttrium content in comparison to the grain composition. Finally the spectra in Fig. 4c (region 2) show the location of a phosphor containing minor phase in composition A-2 whereas this phosphor content is not detectable in composition R-1, which can clearly be seen in the overlaid spectra depicted in Fig. 5. Even though the peak positions of phosphorus and yttrium are close to each other (phosphor Kα at 2.014 keV, yttrium Lα at 1.922 keV) they can be easily distinguished by comparing the peak shapes, i.e. if the yttrium peak contains a shoulder at slightly higher energy, hence the material truly contains phosphorus. It is important to note that neither manganese nor potassium is detectable at any of the observed main and minor phases.

In addition microscopic studies by means of EBSD were performed to figure out if the microstructure is changed with respect to the average grain size and the amount of low sigma grain boundaries. Fig. 6 compares the crystal orientation maps obtained by EBSD of compositions A-1a, A-2a and R-1a (A/B-ratio 0.998) where the low Σ grain boundaries are depicted as white lines between similarly oriented grains (the allowed angular deviation were calculated by Brandon's criterion[50]). Moreover, Table 5 summarizes the average grain size data and the percentage of low Σ grain boundaries both obviously ranging at similar values around 3.4 μm and 6.6% respectively.

The consequences of these microscopic observations with respect to the PTCR characteristics are discussed in Section 4.

3.3. Complex impedance analysis

Impedance measurements, as described in Section 2.3 were carried out for a- and b-compositions between room temperature and 110 °C, i.e. below the ferroelectric to paraelectric phase

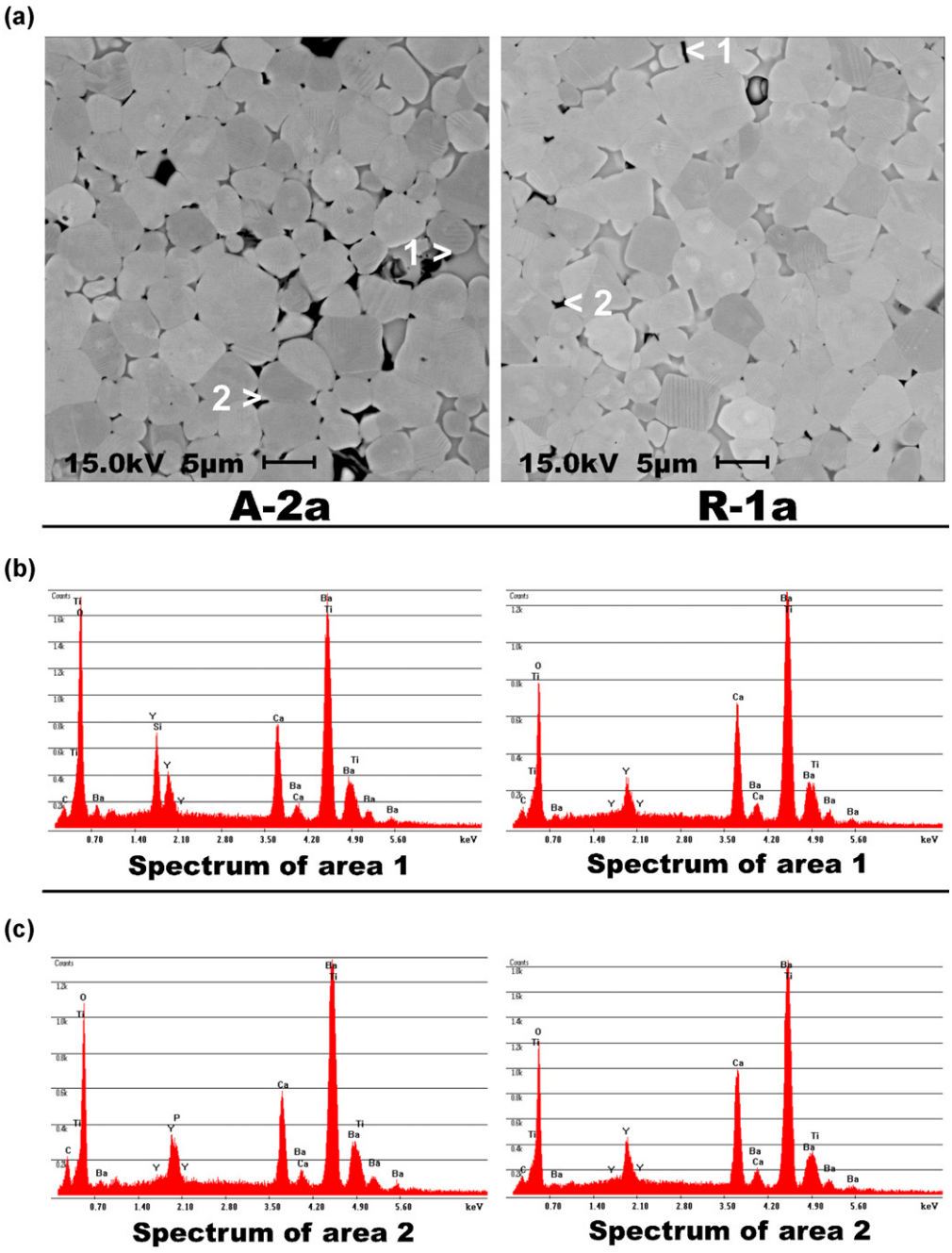

Fig. 4. (a) BSE micrograph (picture width 42.4 μm) and EDX-spectra (b and c) of compositions A-2a and R-1a.

transition at Curie temperature (T_C). The complex plane plots of the impedance data typically consisted of one suppressed semicircle, which was somewhat shifted along the real axis. The impedance spectra were analyzed by means of complex non-linear least squares (CNLS) fitting of the equivalent circuit $L_sR_{bulk}(R_{gb}CPE_{gb})$ (see also insert in Fig. 7a) to the experimental data using the program WinFit (Novocontrol), yielding values for the bulk (R_{bulk}) and grain boundary (R_{gb}) resistances. In addition grain boundary capacitances were extracted from ($R_{gb}CPE_{gb}$), with typical values ranging from 1.9 nF to 15.3 nF (CPE_{gb} is a constant phase element). The inductance of the sample holder, $L_s = 0.5$ μH, was held constant during the fitting procedure.

Fig. 7 shows the resulting complex plane impedance plots (Z'–Z''-plots) (Fig. 7a) and the resistance vs. temperature plot for bulk and grain boundaries (Fig. 7b) of compositions A-1b, A-2b, R-1b as well as A/R-1b and A/R-2b having A/B-ratios of 0.985. The bulk resistances amount typically to 1.5 Ω and 3.5 Ω whereas the grain boundary resistances vary between 3 Ω and 800 Ω.

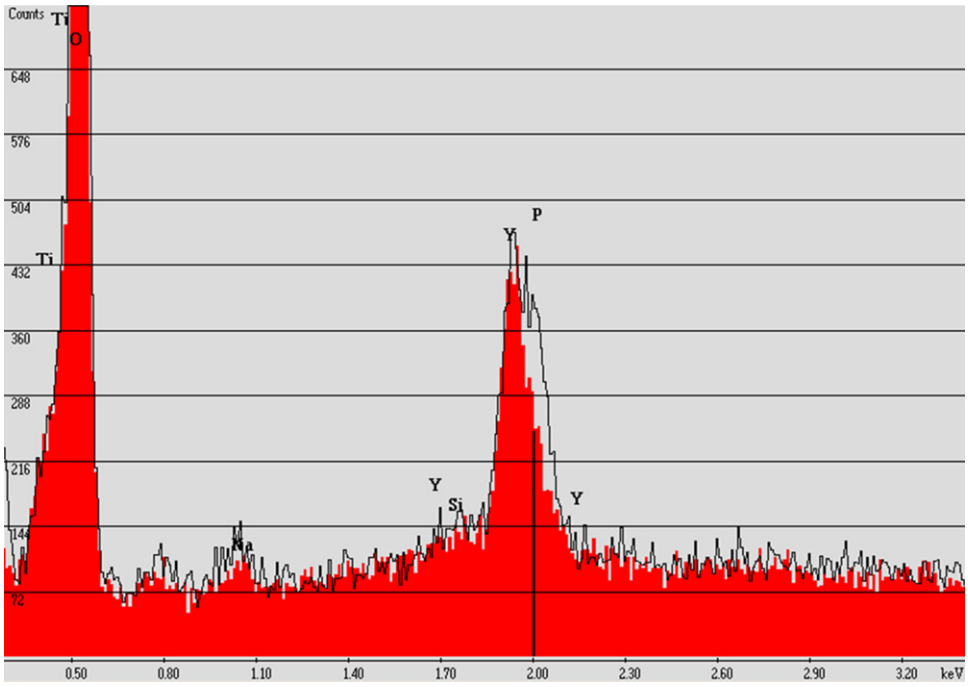

Fig. 5. Overlay of spectra (from Fig. 4c) showing phosphorus in compound A-2a (continuous line spectrum) while no phosphorus is detectable in compound R-1a (filled area spectrum).

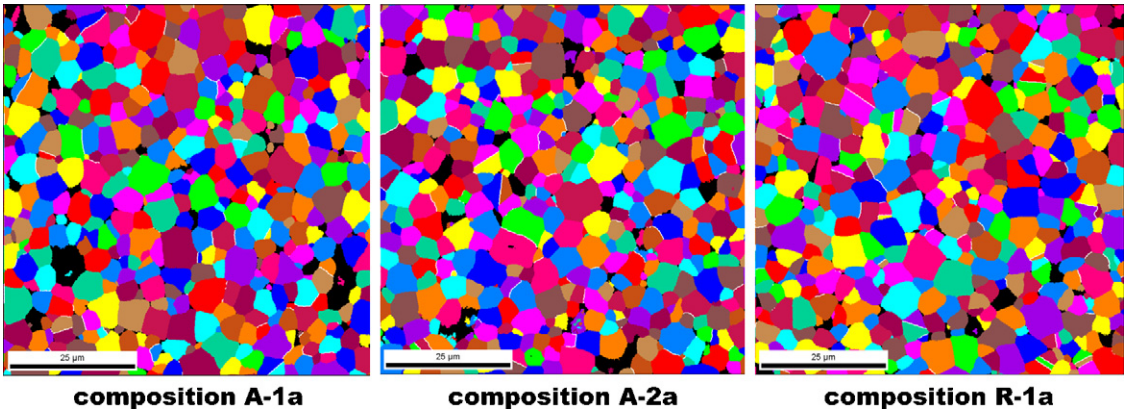

Fig. 6. Crystal orientation (EBSD) maps of compositions A-1a, A-2a and R-1a (left-hand to right-hand).

4. Discussion

According to the results obtained from resistivity measurements (Fig. 1) the purity of the titanium raw material seems to be directly correlated with the resistance, which is further called the impurity effect and is demonstrated in Fig. 8. It indicates that the main impurities of the anatase materials A-1 and A-2, namely phosphor and potassium, give rise to the higher resistance values proving the empirical observations with respect to the applicability of commercial anatase raw materials in PTCR compounds. With the results obtained from composition A/R-1 containing about 89 wt.% anatase and 11 wt.% rutile it is clearly demonstrated that the crystallographic modification of the titanium raw materials in principle does not influence the PTCR performance.

Table 5
Amount of low Σ grain boundaries and average grain size values of composition A-1a, A-2a and R-1a.

Batch no.	Fraction (%)		
Sigma	A-1a	A-2a	R-1a
3	3.5	3.6	3.8
5	1.2	2.2	1.7
9	1.7	1.1	1.1
Remain (%)	93.6	93.1	93.4
Grain size (μm)	3.4	3.3	3.4

The effect of microstructural changes on the electrical characteristics of PTCR-materials is well known in terms of process conditions and dopant effect on anomalous grain growth.[4,5,7,18,38,39,51–55] For example, Drofenik found that anomalous grain growth, which causes the semiconductivity in

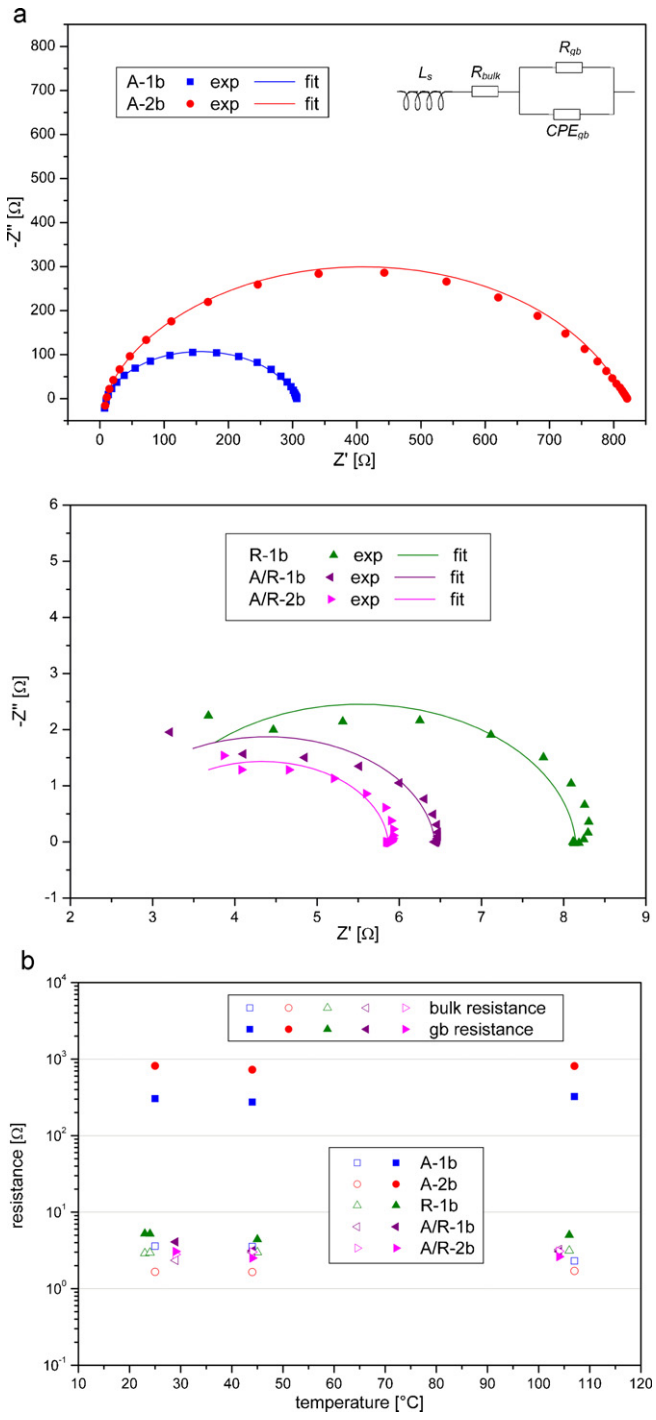

Fig. 7. Impedance analysis of b-compositions: (a) complex plane impedance plot; (b) resistance vs. temperature plot.

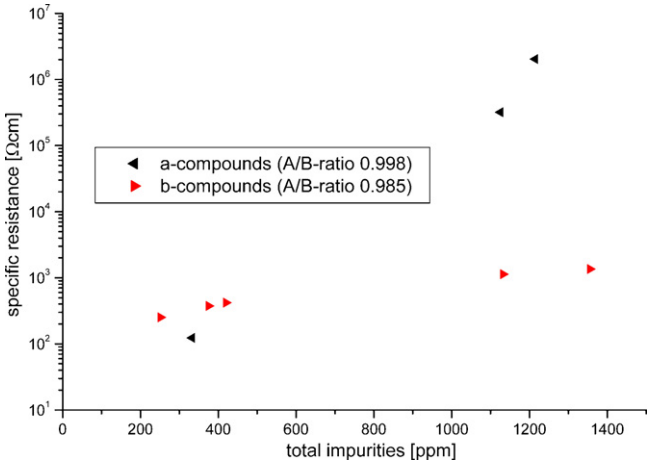

Fig. 8. Correlation of the total impurities with resistivity. Total impurities contain Na, Mg, P, K, Cl, Fe, Zr, Nb (see Table 1).

n-$BaTiO_3$ due to the donor compensating oxygen release during sintering, is a function of the added donor concentration. He also observed that compensating ions such as potassium inhibit this mechanism since such ions act as acceptor dopants. In that case the anomalous grain growth occurs independently of the donor content.[56] For compositions A-1 and A-2 compared to R-1 it is apparent from Figs. 4 and 6 that the microstructural evolution is not affected by the choice of the raw material and in this context is not responsible for the observed high room temperature resistivity in anatase compositions.

Another microstructural feature is known which influences the height and shape of the PTCR-jump, that is to say the number of electrical inactive low Σ grain boundaries.[57–65] Fundamentally low Σ grain boundaries originate from geometric relations between adjacent crystal grains, i.e. such grains periodically share some of the crystal atoms. This relation is theoretically described by the coincident site lattice (CSL) theory for crystalline ensembles.[62] In short this notation means the lower the Σ value the higher is the geometric relation between adjacent grains. The role of low Σ grain boundaries on the PTCR was investigated by several authors since the 1980s, e.g. by Kuwabara et al.[59] or Seaton and Leach.[61] The latter found that low Σ grain boundaries, in particular Σ 3, 5 and 9 boundaries, are inactive with respect to the PTCR-effect hence influencing the steepness of the PTCR characteristics. Seaton and Leach explain this behavior by taking into account that the grain boundary oxidation during cooling from sintering temperature is diminished resulting in lower resistivity above the Curie-temperature, i.e. decreased or suppressed PTCR-jumps or rather a flattened increase of resistivity.

It is evident from the orientation maps obtained by EBSD (Fig. 6) that no significant increase in electrical inactive low sigma grain boundaries is observable (Σ 3, 5 and 9) which was assumed to give reason for the shape of the PTCR characteristics in anatase compositions A-1 and A-2. Summarizing the microscopic results it can be concluded that the microstructure evolution is comparable for the compositions investigated in this work with respect to the average grain size and the evolution of low Σ grain boundaries.

Other studies provide another possibility to explain the observed shifts in PTCR-jump. For example, Jayanthi and Kutty[37] or Ho[34] found that additives such as Al_2O_3, B_2O_3, SiO_2, TiO_2 or BaO influence the activation of defect states due to intergranular secondary phases.[34,35,37] Following Jayanthi and Kutty,[37] who describes the influence of SiO_2-, B_2O_3- and Al_2O_3-addition on the PTCR characteristics of n-$BaTiO_3$, this effect will further be called the effect of segregative addi-

tives. Jayanthi and Kutty[37] detected that B_2O_3 addition causes a steep rise in PTCR-jump whereas Al_2O_3 addition results in flattened resistivity jumps hence shifting R_{max} and T_{max} to higher values. Nevertheless, he also demonstrated that these shifts were clearly distinguishable from the T_C-modification resulting from lead or strontium addition both causing much stronger shifts. Supposing that such an effect also occurs in the compositions prepared from commercial anatase in this study, the observed changes in slope and height of the PTCR-jump might be due to phosphorus containing secondary phase or liquid phase.

With regard to the microstructure observations, which prove the existence of a phosphor containing minor phase (Fig. 4c) located at the grain interspaces, the assumption is made that phosphor is incorporated as segregative additive hence creating another liquid phase. Furthermore the EDXS/WDXS results and the elemental mappings support the presumption made in Section 1 that potassium, with its ionic radius of 1.52 Å ranging close to the barium ionic radius of 1.49 Å, preferentially is incorporated into the grain thus acting as acceptor dopant.

Referring to the microscopic investigations illustrated in Fig. 4a–c one of the remaining questions concerns the role of the Y-containing $CaTiO_3$ minor phase. Due to the results obtained by XRD (Table 3) it is concluded that this phase represents a residual $CaTiO_3$ phase which was assumed to be completely dissolved in the $BaTiO_3$ lattice to form $(Ba,Ca)TiO_3$ solid solution.[66] The mentioned extraordinary high yttrium content (Fig. 4b) detected within the $CaTiO_3$ phase can be explained by taking into account the radii of the involved ions. The ionic radius of the Ba^{2+}-ion is 1.49 Å whereas the ionic radius of Ca^{2+} of 1.14 Å is significantly smaller. Comparing these ionic radii with the donor ion radius of Y^{3+} (1.04 Å) it is apparent why yttrium preferentially is incorporated into the $CaTiO_3$ lattice. Additionally, it is worth noting that during calcination the $CaTiO_3$ formation takes place at temperatures between 560 and 730 °C whereas $BaTiO_3$ forms between 770 and 1033 °C due to the lower decomposition temperatures of $CaCO_3$ compared to $BaCO_3$ (results obtained by thermal analysis using a Netzsch simultaneous TG/DSC). Taking into account the earlier formation and the higher melting point of $CaTiO_3$ as well as the similarity of the ionic radii between calcium and yttrium it becomes more reasonable why such a residual $CaTiO_3$ minor phase acts as a sink for donors.

The observed phase composition gives rise to the presumption that the effective donor concentration, which has to be taken into account when describing the electrical behavior of PTCR-materials, is much lower than it is expected from the nominal composition. Based on a study of the defect chemistry of n-conducting barium titanate at high temperatures (1100–1250 °C), Preis and Sitte[67] estimated the concentrations of point defects for $(Ba_{0.85},Ca_{0.15})TiO_3$ doped with 0.5 mol% yttrium and 0.1 mol% manganese. The donor concentration was found to be approximately 0.22 mol%, which is significantly lower than the nominal value obtained from the overall composition. This discrepancy can not entirely be explained, leaving the open question whether the yttrium dopant is segregated at the grain boundaries or is partly incorporated into the titanium sublattice acting as acceptor ion (partially self compensation of $Y_{Ba}^{\bullet}$ by Y'_{Ti}).

Moreover, Blanchart et al.[68] investigated the grain and grain boundary resistivity in $BaTiO_3$ as a function of yttrium doping by means of impedance spectroscopy and microprobe analysis. They detected that the amount of yttrium incorporated into the $BaTiO_3$ grains is always lower then the overall concentration in the starting powder. Nevertheless, they detected yttrium rich areas inhomogeneously dispersed in the $Ba_6Ti_{17}O_{40}$ minor phase.[68] They did not find any additional intergranular minor phase that dissolves the residual yttrium as is the case in the $(Ba,Ca)TiO_3$ system studied in this work. Referring to these authors and taking into account the microscopic investigations an explanation is now available to resolve the discrepancy between the nominal value and the donor content obtained from defect chemical calculations based on conductivity measurements. It is concluded that the above-mentioned residual $CaTiO_3$ phase dissolves an additional amount of yttrium. Furthermore, it is expected that potassium, introduced by the anatase raw materials, acts as acceptor ion $[K'_{Ba}]$ compensating the donor dopant $Y_{Ba}^{\bullet}$. From these considerations it can be concluded that the effective donor concentration ($[D^{\bullet}]_{eff}$) must be significantly lower than 0.2 mol%, thus increasing the potential barrier. Moreover, in accordance with Eq. (1) a tremendous increase of the Schottky barrier height Φ_0 is anticipated when the interfacial charge density (occupied acceptor state density N_s) is increased probably owing to segregation of acceptor co-dopants and/or impurities.[4,69]

$$\Phi_0 = \frac{eN_s^2}{8\varepsilon_0\varepsilon_r(n_D - n_A)} \quad (1)$$

where e, ε_0 and ε_r denote the elementary charge, the permittivity of vacuum and the relative permittivity. n_D and n_A represent the density of donor and acceptor states present in n-$BaTiO_3$, respectively. It can be deduced from these results that such a decrease of $[D^{\bullet}]_{eff}$ accompanied with an increase of N_s in compositions prepared from sulfate processed anatase TiO_2 (compositions A-1 and A-2) provokes the observed increase of the room temperature resistivity and ρ_{min}, respectively (Fig. 2) by increasing the barrier height, which fits the results of the impedance analysis (Fig. 7). Fig. 7b clearly illustrates that the variation in total resistance, i.e. $R_{gb} + R_b$, and for this reason the DC resistivity (Fig. 1) are only generated by differences in the grain boundary resistance (R_{gb}) and cannot be attributed to changes in bulk resistance (R_b). This indicates that modifications in defect chemistry at the grain boundaries, e.g. the variation in effective donor concentration ($[D^{\bullet}]_{eff}$) or the additional incorporation of acceptor states (N_s), give rise to the higher specific resistance of the anatase compositions A-1 and A-2 as supposed in the Section 1 with respect to the role of the phosphorus and potassium impurities.

5. Conclusion

The effect of commercially anatase TiO_2 raw materials containing the main impurities phosphor and potassium on the PTCR-characteristics of donor and acceptor codoped

(Ba,Ca)TiO_3 ceramics was investigated. It is illustrated that the purity of the titania raw material is responsible for the observed changes in shape and height of the PTCR-jump. Furthermore, it is demonstrated that, if the impurity level of the TiO_2 material is similar, both rutile and anatase generate equal PTCR characteristics verifying that anatase in principle is suitable for PTCR production. Applying microscopic EBSD and EDX/WDX-techniques as well as impedance spectroscopy it is shown that no significant changes in microstructure evolution concerning grain size and low Σ grain boundaries or in chemical composition in terms of the expected main and minor phases are detectable indicating that other effects give rise to the differences in PTCR characteristics. According to these results it is concluded that the variation in PTCR-jump, observed in compositions prepared from commercial anatase TiO_2, results from the combined effect of modified defect chemistry and segregative additives provoked by the impurities present in commercial anatase materials. Referring to the results obtained by impedance analysis and microscopic investigations it is shown that on the one hand potassium is most probably incorporated into the barium sublattice for this reason acting as acceptor (K'_{Ba}) which compensates for the donor dopant $Y_{Ba}^{\bullet}$ thus decreasing the effective donor concentration [$D_{eff}^{\bullet}$]. On the other hand, phosphorus is located in the grain interspaces hence acting as segregative additive.

Acknowledgements

The authors wish to thank EPCOS OHG (Deutschlandsberg, Austria) a Group Company of TDK-EPC Corporation for providing the opportunity to perform this study as well as providing material and technical support.

References

1. Heywang W. Semiconducting barium titanate. *J Mater Sci* 1971;**6**:1214–26.
2. Kulwicki BM. PTC materials technology, 1955–1980. In: Levinson LM, Hill DC, editors. *Advances in ceramics, vol.1. Grain boundary phenomena in electronic ceramics*. Columbus, OH: Am Ceram Soc; 1981. p. 138–54.
3. Waser R. Lineare und nicht-linearеWiderstände. In: Schaumburg H, editor. *Werkstoffe und Bauelemente der Elektrotechnik*. Bd. 5. Stuttgard Teubner; 1994. p. 129–218.
4. Huybrechts B, Ishizaki K, Takata M. Review: the positive temperature coefficient of resistivity in barium titanate. *J Mater Sci* 1995;**30**:2463–74.
5. Ueoka H, Yodogawa M. Ceramic manufacturing technology for the high performance PTC thermistor. *IEEE Trans Manuf Technol* 1974;**3**:77–82.
6. Ihrig H. PTC effect in $BaTiO_3$ as a function of doping with 3d elements. *J Am Ceram Soc* 1981;**64**:617–20.
7. Ting C-J, Peng C-J, Lu H-Y, Wu S-T. Lanthanum–magnesium and lanthanum–manganese donor–acceptor-codoped semiconducting barium titanate. *J Am Ceram Soc* 1990;**73**:329–34.
8. Yoon SH, Lee KH, Kim H. Effect of acceptors on the segregation of donors in niobium-doped barium titanate positive temperature coefficient resistors. *J Am Ceram Soc* 2000;**83**:2463–72.
9. Barksdale J. *Titanium; its occurrence, chemistry and technology*. New York: Ronald Press; 1949.
10. Czanderna AW, Clifford AF, Honig JM. Preparation of highly purified TiO_2 (anatase). *J Am Chem Soc* 1957;**79**:5407–9.
11. Suzuki A, Kotera Y. The kinetics of the transition of titanium dioxide. *Bull Chem Soc Jpn* 1962;**35**:1353–7.
12. Yoganarasimhan SR, Rao CNR. Mechanism of crystal structure transformations. Part 3: factors affecting the anatase–rutile transformation. *Trans Faraday Soc* 1962;**58**:1579–89.
13. Suzuki A, Tukuda R. Kinetics of the transition of titanium dioxide prepared by sulfate process and chloride process. *Bull Chem Soc Jpn* 1969;**42**:1853–7.
14. Hadjivanov KI, Klissurski DG, Davydov AA. Study of phosphate-modified TiO_2-anatase. *J Catal* 1989;**116**:498–505.
15. Barnard AS, Zapol P. Effects of particle morphology on surface hydrogenation on the phase stability of TiO_2. *Phys Rev B* 2004;**70**:235403.
16. Barnard A, Curtiss L. Prediction of TiO_2 nanoparticle phase and shape transitions controlled by surface chemistry. *Nanoletters* 2005;**5**: 1261–6.
17. Heywang W, Brauer H. Zum Aufbau der Sperrschichten in kaltleitendem Bariumtitanat. *Solid-State Electron* 1965;**8**:129–35.
18. Lee S, Randall CA, Liu Z-K. Factors limiting equilibrium in fabricating a simple ferroelectric oxide: $BaTiO_3$. *J Am Ceram Soc* 2009;**92**: 222–8.
19. Ryu S-S, Yoon D-H. Solid-state synthesis of nano-sized $BaTiO_3$ powder with high tetragonality. *J Mater Sci* 2007;**42**:7093–9.
20. Spieß G. Über die Bildung von Bariummetatitanat. *Ber DKG* 1961;**38**:495–528.
21. Kubo T, Kato M, Fujita T. Solid state reactions between TiO_2 and $BaCO_3$. *Kogyo Kagaku Zasshi* 1967;**70**:847–53.
22. Suyama Y, Kato A. Reactivity of ultrafine-TiO_2 (anatase) powders with $BaCO_3$. *Ceram Int* 1975;**1**:5–9.
23. Suyama Y, Kato A. Solid-state reactions between CVD-TiO_2 and $BaCO_3$. *Bull Chem Soc Jpn* 1977;**50**:1361–6.
24. Beauger A, Mutin JC, Niepce JC. Synthesis reaction of metatitanate $BaTiO_3$. Part 1: effect of the gaseous atmosphere upon the thermal evolution of the system $BaCO_3$–TiO_2. *J Mater Sci* 1983;**18**:3041–6.
25. Amin A, Spears MA, Kulwicki BM. Reaction of anatase and rutile with barium carbonate. *J Am Ceram Soc* 1983;**66**:733–8.
26. Fernandez JF, Duran P, Moure C. Dielectric and microstructural properties of sintered $BaTiO_3$ ceramics prepared from different TiO_2 raw materials. *J Mater Sci* 1991;**26**:3257–63.
27. Tsutai S, Hayashi T, Hayashi S, Nakagawa Z. Reaction mechanism of $BaTiO_3$ from powder compacts, $BaCO_3$ and TiO_2 and expansion phenomenon during formation process. *J Chem Soc Jpn* 2001;**109**:1028–34.
28. Brzozowski E, Sanchez J, Castro MS. $BaCO_3$–TiO_2 solid state reaction: a kinetic study. *J Mater Syn Process* 2002;**10**:1–5.
29. Fukami T, Tsuchiya H. Dependence of resistivity on donor dopant content in barium titanate ceramics. *Jpn J Appl Phys* 1979;**18**:735–8.
30. Glinchuk M, Bykov IP, Kornienko SM, Laguta VV, Slipenyuk AM, Bilous AG, et al. Influence of impurities on the properties of rare-earth-doped barium titanate ceramics. *J Mater Chem* 2000;**10**:941–7.
31. Ueoka H. The doping effects of transition elements on the PTC anomaly of semiconductive ferroelectric ceramics. *Feroelectrics* 1974;**7**:351–3.
32. Kuwabara M, Kumamoto K. PTCR characteristics in barium titanate ceramics with Curie points between 60° and 360 °C. *J Am Ceram Soc* 1983;**66**:C214–5.
33. Tseng TY, Wang SH. AC electrical properties of high-Curie-point barium-lead titanate PTCR ceramics. *Mater Lett* 1990;**9**:164–8.
34. Ho I-C. Semiconducting barium titanate ceramics prepared by boron-containing liquid-phase sintering. *J Am Ceram Soc* 1994;**77**: 829–32.
35. Kutty TRN, Hari NS. Effect of charge redistribution through secondary phase formation on PTCR characteristics of n-$BaTiO_3$ ceramics. *Mater Lett* 1998;**34**:43–9.
36. Yoon S-H, Lee J-H, Kim D-Y, Hwang NM. Effect of liquid-phase characteristic on the microstructure and dielectric properties of donor-(niobium) and acceptor-(magnesium)doped barium titanate. *J Am Ceram Soc* 2003;**86**:88–92.
37. Jayanthi S, Kutty TRN. Effect of segregative additives on the positive temperature coefficient in resistance characteristics of n-$BaTiO_3$ ceramics. *J Mater Sci: Mater Electron* 2006;**17**:883–97.
38. Sauer HA, Fischer JR. Processing of positive temperature coefficient thermistors. *J Am Ceram Soc* 1960;**43**:297–301.

39. Daniels J, Wernicke R. Doped barium titanate ceramics. Part V: new aspects of an improved PTC model. *Philips Res Rep* 1976;**31**:544–59.
40. Preis W, Sitte W. Modelling of grain boundary resistivities of n-conducting $BaTiO_3$ ceramics. *Solid State Ionics* 2006;**177**:2549–53.
41. Scholze H. *Glass: nature structure and properties*. 3rd ed. Berlin: Springer; 1990.
42. Vogel W. *Glaschemie*. 3rd ed. Berlin: Springer; 1992.
43. Caballero AC, Fernandez JF, Duran P, Moure C. Phosphor-doped $BaTiO_3$: microstructure development and dielectric properties. *J Mater Sci* 1995;**30**:3799–804.
44. Wang X-H, Gui Z-L, Li L-T. Effect of phosphor doping on the microstructure and dielectric properties of barium titanate ceramics. *Mater Chem Phys* 1998;**55**:193–6.
45. Caballero AC, Fernandez JF, Moure C, Duran P. Phase formation in phosphorus doped $BaTiO_3$. *Mater Lett* 1998;**35**:72–7.
46. Caballero AC, Fernandez JF, Villegas M, Moure C, Duran P. Intermediate phase development in phosphorus-doped barium titanate. *J Am Ceram Soc* 2000;**83**:1499–505.
47. Niimi H, Mihara K, Sakabe Y. Influence of Ba/Ti ratio on the positive temperature coefficient of resistivity characteristics of Ca-doped semiconducting $BaTiO_3$ fired in reducing atmosphere and reoxidized in air. *J Am Ceram Soc* 2007;**90**:1817–21.
48. Sakabe Y. Development of dielectric ceramics for nickel electrode multilayer capacitors. *J Jpn Soc Powder Powder Metall* 2004;**51**: 274–84.
49. Heuschmann M. Einfluss der Stöchiometrie auf die elektrischen Eigenschaften ausgewählter PTC Massen. Diploma thesis. Nürnberg: Georg-Simon-Ohm University of Applied Science Nürnberg (faculty of material science), 2006.
50. Brandon DG. The structure of field-evaporated surfaces. *Surf Sci* 1965;**3**:1–18.
51. Drofenik M. Oxigen partial pressure and grain growth in donor-doped $BaTiO_3$. *J Am Ceram Soc* 1987;**70**:311–4.
52. Peng C-J, Lu H-Y. Compensation effect in semiconducting barium titanate. *J Am Ceram Soc* 1988;**71**:C44–6.
53. Drofenik M. Initial specific surface area and grain growth in donor-doped barium titanate. *J Am Ceram Soc* 1990;**73**:1587–92.
54. Drofenik M. Origin of the grain growth anomaly in donor-doped barium titanate. *J Am Ceram Soc* 1993;**76**:123–8.
55. Drofenik M, Makovec D, Zajc I, Langhammer HT. Anomalous grain growth in donor-doped barium titanate with excess barium oxide. *J Am Ceram Soc* 2002;**85**:653–60.
56. Drofenik M. Grain growth during sintering of donor-doped barium titanate. *J Am Ceram Soc* 1986;**69**:C8–9.
57. Nemoto H, Oda I. Direct examination of PTC action of single grain boundaries in semiconducting $BaTiO_3$ ceramics. *J Am Ceram Soc* 1980;**63**:398–401.
58. Ogawa H, Demura M, Yamamoto T, Sakuma T. Estimation of PTCR effect in single grain boundary of Nb-doped BaTiO3. *J Mater Sci Lett* 1995;**14**:537–8.
59. Kuwabara M, Morimo K, Matsunaga T. Single-grain boundaries in PTC resistors. *J Am Ceram Soc* 1996;**79**:997–1001.
60. Hayashi K, Yamamoto T, Sakuma T. Grain orientation dependence of the PTCR effect in niobium-doped barium titanate. *J Am Ceram Soc* 1996;**79**:1669–972.
61. Seaton J, Leach C. Evolution of low sigma grain boundaries in PTC thermistors during sintering. *J Eur Ceram Soc* 2005;**25**:3055–8.
62. Gertsman VY. Coincide site lattice theory of multicrystalline ensembles. *Acta Cryst A* 2001;**57**:649–55.
63. Randle V, Hu Y. The role of vicinal $\Sigma 3$ boundaries and $\Sigma 9$ boundaries in grain boundary engineering. *J Mater Sci* 2005;**40**:3243–6.
64. Blamey JM, Parry TV. The effect of processing variables on the mechanical and electrical properties of barium titanate positive temperature coefficient-of-resistance ceramics. Part I: additives and processing prior to sintering. *J Mater Sci* 1993;**28**:4311–6.
65. Yoo Y-S, Kim H, Kim D-Y. Effect of SiO_2 and TiO_2 addition on the exaggerated grain growth of $BaTiO_3$. *J Eur Ceram Soc* 1997;**17**:805–11.
66. DeVries RC, Roy R. Phase equilibria in the system $BaTiO_3$–$CaTiO_3$. *J Am Ceram Soc* 1955;**38**:142–6.
67. Preis W, Sitte W. Electronic conductivity and chemical diffusion in n-conducting barium titanate at high temperatures. *Solid State Ionics* 2006;**177**:3093–8.
68. Blanchart P, Baumard JF, Abelard P. Effect of yttrium doping on the grain and grain-boundary resistivities of $BaTiO_3$ for positive temperature coefficient thermistors. *J Am Ceram Soc* 1992;**75**:1068–72.
69. Preis W, Bürgermeister A, Sitte W, Supancic P. Bulk and grain boundary resistivities of donor-doped barium titanate ceramics. *Solid State Ionics* 2004;**173**:69–75.